Article:

Penotti, Fabio E., Cooper, David L. and Karadakov, Peter Borislavov orcid.org/0000-0002-2673-6804 (2021) The Role of Dynamical Electron Correlation in the Differences inBonding Between CaAlH3 and MgAlH3. Journal of Physical Chemistry A. pp. 3912-3919. ISSN 1089-5639

https://doi.org/10.1021/acs.jpca.1c02422

The Role of Dynamical Electron Correlation in the Differences in Bonding Between $CaAlH_3$ and $MgAlH_3$

Fabio E. Penotti,*,† David L. Cooper,*,‡ and Peter B. Karadakov§

†Consiglio Nazionale delle Ricerche Istituto di Scienze e Tecnologie Chimiche “Giulio Natta”, Via Golgi 19, I–20133 Milano MI, Italy
‡Department of Chemistry, University of Liverpool, Liverpool L69 7ZD, UK
§Department of Chemistry, University of York, Heslington, York YO10 5DD, UK

alkaline earth metal atoms – aluminium hydride – electron correlation – spin-coupled generalized valence bond theory – M'AlH₃.

Corresponding authors: Fabio E. Penotti – Email: f.penotti@gmail.com; David L. Cooper – Email: dlc@liverpool.ac.uk

ABSTRACT: The most important factor behind the intriguing differences between the geometries of the $M'AlH_3$ ($M' = Mg$, Ca) molecules is shown to be dynamical electron correlation and not intramolecular Coulombic interactions, as previously thought. Spin-coupled generalized valence bond (SCGVB) calculations reveal the different bonding situations in the two molecules at their optimal geometries but do not explain why these geometries differ so much; the solution to this conundrum comes instead from detailed analysis of coupled-cluster (CCSD(T)) energies at model and optimal geometries.

INTRODUCTION

Especially for the ground electronic states of small closed-shell neutral molecules constructed only from main group atoms, for which simple models such as VSEPR (Valence Shell Electron Pair Repulsion) and its various extensions usually work well,[1-5] it is not very often that dynamical electron correlation is a factor that plays an important role in determining the shape of a neutral molecule and the nature of its bonding in the electronic ground state. We believe that we have identified particularly clear examples of such molecular systems.

Anusiewicz et al.[6] have recently discovered surprising geometrical features for certain C_{3v} $M'MH_3$ species in which M′ is an alkaline earth atom and M is B, Al or Ga. As M′ approaches a planar MH_3 unit along its C_3 axis a reasonable expectation is of course that some degree of donation would develop of $M'(s^2)$ valence electrons into the vacant $MH_3(p)$ orbital. The basic geometric arrangement that would then be anticipated for such a C_{3v} complex is as shown in Figure 1, in which θ, the deviation of the M′MH bond angle from 90°, is expected to be relatively small and positive, perhaps on the order of +4°, so that the H atoms are directed away from M′. This is indeed what has been found when M′ is Mg but Anusiewicz et al.[6] observed for the interaction of Ca with AlH_3 or GaH_3 that the resulting neutral C_{3v} complexes have values of θ which are significantly negative, typically on the order of −35°, so that the H atoms are instead directed towards M′, see Figure 1 and Table 1. (Instead of this easily visualized ‘umbrella angle’ θ we could of course have specified these geometries in terms of the HMHH dihedral angle, in an analogous fashion to interesting previous work on stable anions of $M'BH_3$ systems.[7])

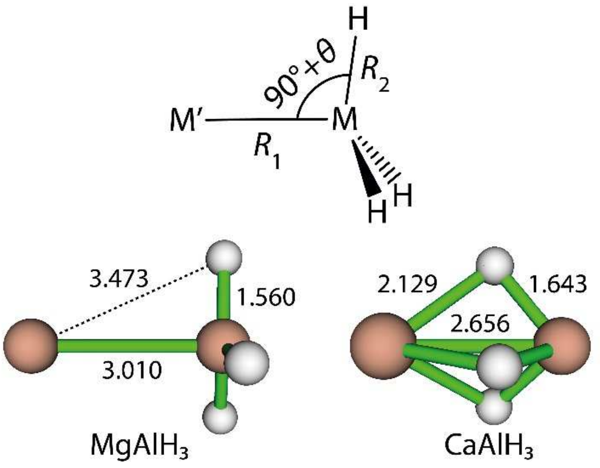

Figure 1. Definition of the geometric parameters R_1, R_2 and θ for C_{3v} $M'MH_3$ species; CCSD(T)/aug-cc-pVQZ geometries of $MgAlH_3$ and $CaAlH_3$ (see Table 1) with interatomic distances (Å).

Much of the specific interest in $MgAlH_3$ and $CaAlH_3$ has been derived from the fact that such molecules correspond to straightforward functionalizations of alane (AlH_3) which has numerous applications in organic synthesis as a reducing agent for specific functional groups,[8] and which is also used as a rocket fuel additive.[9] Theoretical research on $MgAlH_3$ and $CaAlH_3$ can be traced back to the late 1980s.[10, 11] For challenges to theory that are presented by these molecules, see Ref. 12.

The initial idea behind the present work was to use spin-coupled generalized valence bond (SCGVB) calculations for $MgAlH_3$ (small positive θ) and $CaAlH_3$ (significantly negative θ) to understand *how* the bonding situation differs at these two rather different geometrical arrangements. As part of a first attempt to understand *why* these two systems prefer such different geometries we also decided to re-examine a suggestion of Anusiewicz et al.[6] that associated the special geometric characteristics of the Ca systems with an enhanced Coulombic interaction energy between the atomic partial charges. We find, however, that an explanation for the somewhat different geometries is more likely to lie elsewhere.

The structure of this paper is as follows. We outline in the next section the various computational methods that we used. We then present our results and discussion, starting with geometry optimizations and calculations of Coulombic interaction energies between atomic partial charges, before demonstrating how SCGVB theory reveals but does not explain key differences between the two bonding situations, and then identifying an underlying cause for the different optimal geometric arrangements of $M'AlH_3$ (M' = Mg, Ca).

COMPUTATIONAL METHODS

Using standard all-electron aug-cc-pVTZ basis sets, the geometries of $MgAlH_3$ and $CaAlH_3$ were optimized at the CCSD(T) level, correlating all of the electrons. All vibrational frequencies were found to be real, confirming that we had indeed located local minima. The resulting geometric parameters turned out, unsurprisingly, to be similar to those reported by Anusiewicz et al.[6] To enable fair comparisons of the bonding situations in $MgAlH_3$ and $CaAlH_3$, we also optimized model geometries for both systems, with θ fixed at −35° for $MgAlH_3$ and at +4° for $CaAlH_3$. The various CCSD(T) geometry optimizations, which were all carried out using MOLPRO,[13-15] were subsequently repeated using instead standard aug-cc-pVQZ basis sets, as stored internally by MOLPRO. In particular, the aug-cc-pVQZ basis set for Ca is the one constructed by Hill and Peterson.[16]

Atomic populations were generated at the various CCSD(T)/aug-cc-pVQZ geometries by means of CCSD/aug-cc-pVQZ calculations. From the plethora of rival approaches we chose to use natural population analysis (NPA) partial charges obtained with the natural bond order (NBO) analysis facilities in Gaussian 16[17] and Voronoi deformation density (VDD) charges,[18] as implemented in version 3.6 of Multiwfn.[19] Given that some numerical partial charges (such as those from the standard Mulliken scheme) can be unreliable when using large basis sets with diffuse functions, we decided to use not only aug-cc-pVQZ but also (for the same geometries) the much more modest 6-31G** basis sets that are available at the Basis Set Exchange.[20] (Note that for 6-31G** we used basis functions in spherical rather than Cartesian form.)

The spin-coupled generalized valence bond (SCGVB) wave functions used here for the eight valence electrons of $M'AlH_3$ (M' = Mg, Ca) take the form

$$\Psi_{\mathrm{SCGVB(8)}} = \hat{\mathcal{A}}\left[(\text{closed-shell})\ \varphi_1\varphi_2\cdots\varphi_8\ \Theta^8_{0,0}\right] \qquad (1)$$

in which the eight singly-occupied nonorthogonal active orbitals, φ_i, are fully optimized, without any locality constraints, and the total active space spin function, $\Theta^8_{0,0}$, is simultaneously optimized as a linear combination of all 14 Kotani spin functions which couple the spins of these eight electrons to yield a state with $S = 0$ and $M_S = 0$.[21] Purely for convenience, the doubly-occupied inactive closed-shell orbitals for the various SCGVB/aug-cc-pVQZ calculations were taken, without further optimization, from the corresponding CASSCF(8,8)/aug-cc-pVQZ wave functions. We checked that adopting instead RHF or CASSCF(8,11) inactive orbitals leads only to rather trivial changes in the results obtained.

All of the various CASSCF calculations were carried out using the GAMESS-US package[22, 23] and the SCGVB calculations were performed using the generalized multiconfiguration spin-coupled (GMCSC) program developed by Penotti,[24-27] taking the required integrals over basis functions from GAMESS-US. Pictorial depictions of the resulting SCGVB orbitals were generated using Multiwfn[19] which was also used for the quantum theory of atoms in molecule (QTAIM) analysis[28] and, as noted above, for the calculations of VDD partial charges.[18]

RESULTS AND DISCUSSION

The fully-optimized C_{3v} geometries obtained at the CCSD(T) level using aug-cc-pVTZ and aug-cc-pVQZ basis sets (see Table 1) reproduce a key finding of Anusiewicz et al.:[6] in contrast to the optimal geometry for $MgAlH_3$ which has a fairly conventional small positive value for θ of *ca*. +4°, the corresponding angle for $CaAlH_3$ is significantly negative (*ca*. −35°). As can be seen from Table 1, switching from aug-cc-pVTZ to the larger aug-cc-pVQZ basis set leads for $MgAlH_3$ to small reductions in the values of the AlH distance, R_2, and the angle, θ, with a small increase in the MgAl distance, R_1. It turns out that our two sets of geometric parameters for $MgAlH_3$ straddle those reported previously.[6] The corresponding improvement in the basis set for $CaAlH_3$ leads to small reductions in R_1 and R_2, with a parallel increase in θ. Although here again the two sets of R_1 and θ values straddle those reported previously[6] which were based on calculations that used a pseudopotential for Ca, our values of R_2 turn out to be slightly smaller.

Whereas the optimal C_{3v} geometry of $MgAlH_3$ is characterized by a relatively large MgAl separation, that for $CaAlH_3$ features a relatively short CaAl separation as well as AlH distances that are slightly longer than in $MgAlH_3$. As a first step towards trying to understand these differences we constructed a model geometry for $MgAlH_3$ in which θ was fixed at −35° (comparable to that in the optimal structure for $CaAlH_3$). According to CCSD(T)/aug-cc-pVTZ calculations, the energetic cost relative to the fully-optimized geometry of fixing θ in this way, without reoptimization of R_1 and R_2, is 23.6 kcal/mol. Keeping these fixed values of R_2 and θ we then reoptimized R_1, finding a somewhat smaller value of 2.435 Å, accompanied by an energy lowering of 15.5 kcal/mol. Finally, we reoptimized both of R_1 and R_2 with θ still fixed at −35°. This resulted in only a very small additional change in R_1, but in a significant increase in R_2 to 1.693 Å and an energy lowering of 3.6 kcal/mol. It is striking that the resulting geometry (see Table 1) features AlH distances that are now much the same as those in $CaAlH_3$ and that the MgAl separation is also now somewhat smaller than that for the optimal geometry. Overall, we find at this level of theory that the fully-optimized geometry for $MgAlH_3$ is preferred relative to the optimized model structure with fixed $\theta = -35°$ by 4.5 kcal/mol. (Note that we have simply compared the CCSD(T) energies, without attempting any corrections for differences in the zero-point vibrational energies for different θ values. The various CCSD(T) energies for all these geometries are reported in Table S1 in the Supporting Information.)

Table 1. Geometric Parameters (as Defined in Figure 1) Optimized at the CCSD(T) Level for $MgAlH_3$ and $CaAlH_3$ with Different Basis Sets. The Values Labelled 'Literature' are Taken from Anusiewicz et al.[6]

	aug-cc-pVTZ	aug-cc-pVQZ	Literature
$MgAlH_3$			
R_1/Å	2.953	3.010	3.003
R_2/Å	1.589	1.560	1.587
θ	+3.92°	+3.46°	+3.78°
$CaAlH_3$			
R_1/Å	2.749	2.656	2.737
R_2/Å	1.697	1.643	1.706
θ	−34.81°	−36.74°	−35.29°
$MgAlH_3$ (model)			
R_1/Å	2.440	2.380	
R_2/Å	1.693	1.641	
θ (fixed)	−35°	−35°	
$CaAlH_3$ (model)			
R_1/Å	3.280	3.175	
R_2/Å	1.593	1.564	
θ (fixed)	+4°	+4°	

It did of course seem rather worthwhile to repeat this exercise for $CaAlH_3$, this time changing θ to a fixed value of +4° (comparable to that in the optimal structure for $MgAlH_3$). It was our expectation that the AlH distances (R_2) would end up being similar to those observed for the optimal $MgAlH_3$ structure and also that the CaAl distance (R_1) would become somewhat longer than in the optimal $CaAlH_3$ structure. According to the CCSD(T)/aug-cc-pVTZ calculations, the energetic cost for $CaAlH_3$ of fixing $\theta = +4°$ without reoptimization of R_1 and R_2 is 21.3 kcal/mol. Subsequent optimization of R_1 with fixed θ and R_2 leads to an energy lowering of 6.6 kcal/mol, with $R_1 = 3.244$Å. Finally, fixing only $\theta = +4°$, we find $R_1 = 3.280$Å, $R_2 = 1.593$Å and a further energy improvement of 4.2 kcal/mol. All in all, our expectations have been realized (see Table 1): the AlH distances for the model geometry of $CaAlH_3$ with fixed $\theta = +4°$ are similar to those in the optimal $MgAlH_3$ structure and, similarly, the CaAl separation is somewhat larger than in the optimal geometry of $CaAlH_3$. Overall, at this level of theory, the optimal geometry for $CaAlH_3$ turns out to be preferred relative to the optimized model structure with fixed $\theta = +4°$ by 10.5 kcal/mol (again simply comparing the CCSD(T) energies).

Also shown in Table 1 are the corresponding model geometries for $MgAlH_3$ and $CaAlH_3$ that were generated using instead CCSD(T)/aug-cc-pVQZ calculations. (The various energies are reported in Table S1 in the Supporting Information.) The overall patterns in the values of R_1 and R_2 are clearly the same as we observed with the smaller basis set. For the $M'AlH_3$ geometries with $\theta \sim +4°$, switching M′ from Mg to Ca has little effect on the AlH distances, but it increases the M′Al separation by 0.16 Å–0.33 Å, depending on the quality of the basis set. Comparing instead the two geometries with $\theta \sim -35°$, it is clear that switching M′ from Mg to Ca again has little effect on the (slightly longer) AlH distances but it increases the M′Al separation by *ca*. 0.3 Å.

We could of course imagine that the process of forming $M'AlH_3$ involves an initial symmetrical distortion of AlH_3, so as to adopt the same geometry as in the $M'AlH_3$ complex, and then the further changes due to the interaction of this deformed AlH_3 unit with the M′ atom. It is clear from the CCSD(T)/aug-cc-pVQZ energies of various geometries of symmetrically distorted AlH_3 (as reported in Table S2 in the Supporting Information) that most of the deformation energy is associated with the change in θ rather than with the increased AlH separation. Comparing the CCSD(T)/aug-cc-pVQZ energies for $M'AlH_3$ (as listed in Table S1 in the Supporting Information, without any corrections for vibrational energies), we find that our model geometry for $MgAlH_3$ with $\theta = -35°$ is disfavored relative to the optimal one with $\theta \sim +4°$ by 4.6 kcal/mol. In this case a cost of 58.8 kcal/mol for further distortion of the AlH_3 moiety is only partially compensated by an increase in the interaction energy with the Mg atom of 54.1 kcal/mol. The situation is of course entirely different in $CaAlH_3$, for which the optimal geometry with $\theta \sim -35°$ is favored relative to the model geometry ($\theta = +4°$) by 21.1 kcal/mol at this level of theory. It turns out that this overall energy difference corresponds to a cost of 64.7 kcal/mol for the further distortion of the AlH_3 moiety being more than compensated by an increase of 85.8 kcal/mol for the interaction energy with the Ca atom. Relative to the situation for $\theta \sim +4°$, the enhanced interaction for $\theta \sim -35°$ between the deformed AlH_3 moiety and the M′ atom clearly increases by more than 50% (54.1 to 85.8 kcal/mol) upon switching from Mg to Ca.

Investigating the energetic differences between $MgAlH_3$ and $CaAlH_3$, Anusiewicz et al.[6] used sets of point charges located at nuclear positions in order to assess the relative values of the Coulombic attraction energies between positively and negatively charged centers. Using their M′H separations and the NPA partial charges obtained from NBO analysis, they showed that the Coulombic interaction energy between the net positive charge on the M′ atom and the net negative charges on each of the three H atoms is substantially more favorable for $CaAlH_3$ with $\theta \sim -35°$ than it is for $MgAlH_3$ with $\theta \sim +4°$. They identified this difference as being key for rationalizing the preference shown by $CaAlH_3$ for the geometry with significantly negative θ. Certainly this special geometric characteristic does enhance the Coulombic attraction between the net positive charge on the Ca atom and the net negative charges on the H atoms. All of this is of course entirely plausible but, nonetheless, it is informative also to compare two M′AlH$_3$ species that have much the same value of θ, whether it is $\sim +4°$ or $\sim -35°$. With this in mind, we decided for our various CCSD(T)/aug-cc-pVQZ geometries to use atomic populations (CCSD level), together with the calculated M′Al and M′H distances, so as to assess the relative values of Coulombic interaction energies, in a very similar fashion to Anusiewicz et al.[6]

Comparing the atomic populations (CCSD level) calculated using aug-cc-pVQZ and 6-31G** basis sets, we observe that the NPA charges show only modest basis set dependence and the same is true for the VDD charges, but that the corresponding sets of VDD and NPA charges are nonetheless rather different from one another (see Table S3 in the Supporting Information). The NPA charge on Al is typically on the order of about double the corresponding VDD charge and, at the $\theta \sim -35°$ geometries, the NPA charge on M′ is on the order of about three times the corresponding VDD charge. The Mulliken charges (6-31G** basis set) resemble most those from the VDD scheme. We then examined the simple point-charge Coulombic energies both for the interaction of M′ with just the three H atoms, as was done by Anusiewicz et al.,[6] and also for the interaction of M′ with all of the AlH$_3$ moiety.

Clearly the significant differences between the NPA and VDD (or Mulliken) estimates of the degree of charge separation must have a big impact on the calculated Coulombic energies. Nonetheless we find consistently, whether we consider the M′…H$_3$ or M′…AlH$_3$ interactions, that these Coulombic interactions are indeed more attractive for CaAlH$_3$ with $\theta \sim -35°$ than they are for MgAlH$_3$ with $\theta \sim +4°$ (see Tables S4 and S5 in the Supporting Information). Unsurprisingly, the magnitude of this preference varies significantly with the particular choice of partial charges. However, we also observe for the two M′AlH$_3$ geometries with $\theta \sim +4°$ that the Coulombic interaction energies are mostly rather similar to one another for any given mode of calculation. It turns out that such an observation also holds to a fair degree for the M′AlH$_3$ geometries with $\theta \sim -35°$. On the whole, the change in θ appears to be far more important for the Coulombic interaction energy between atomic partial charges than is changing the M′ atom. As a consequence, even without repeating this simple analysis with many different sets of partial charges, it does unfortunately already seem slightly questionable to invoke differences in M′…H$_3$ Coulombic attractions when rationalizing the preference of the Mg system for small positive θ and of its Ca counterpart for significantly negative θ.

In order to reveal how the bonding situations differ between MgAlH$_3$ and CaAlH$_3$ at their optimal CCSD(T)/aug-cc-pVQZ geometries, we then turned to the results of SCGVB/aug-cc-pVQZ calculations. The description that emerges for MgAlH$_3$ at its optimal geometry features three symmetry-equivalent pairs, one for each AlH bond, with in each case one orbital (see φ_1 in top row of Figure 2) that is semi-localized on H whereas the corresponding Al-based orbital (see φ_2 in top row of Figure 2) shows rather significant deformation towards H, consistent with the electronegativity differences. The two orbitals in each pair have an overlap of 0.81 (see Table 2) and the corresponding electron spins are overwhelmingly singlet coupled. Taken together, these observations indicate the presence of three somewhat unsurprising AlH bonds, very much as we might have expected for this geometrical arrangement. There are much smaller overlaps (see Table 2) between SCGVB orbitals that are associated with different AlH bonds. To a first approximation, we observe from the forms of orbitals φ_7 and φ_8 that the doubly-occupied Mg(3s^2) orbital splits into separate s$_-$ and s$_+$ lobe orbitals which are concentrated in opposite directions along the C$_3$ axis. Unlike the s$_-$ orbital, which is concentrated away from Al (see φ_8 in top row of Figure 2) and mostly retains its basic form, the corresponding s$_+$ function deforms/distorts significantly towards the Al center (see φ_7 in top row of Figure 2) thereby also transferring charge to the AlH$_3$ moiety. Orbitals φ_7 and φ_8 do, though, retain an overlap of 0.59. The overall active space spin function is dominated by the perfect pairing mode of spin coupling, with a weight of a little more than 99.7%.

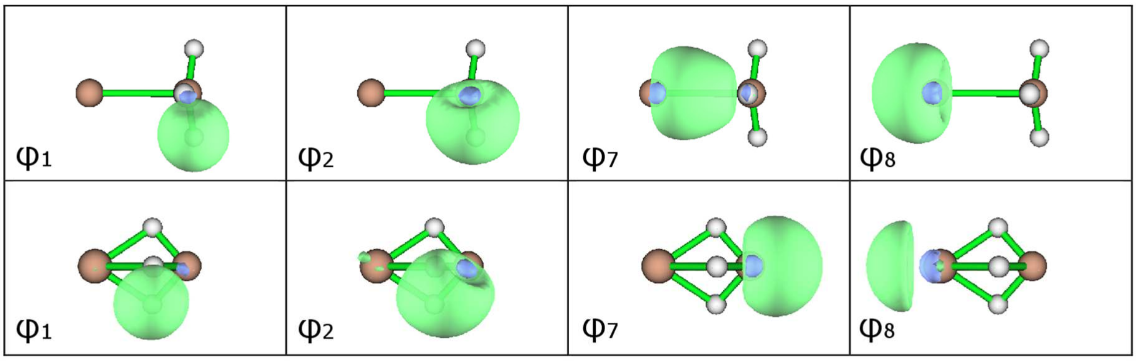

Figure 2. Symmetry-unique SCGVB orbitals for MgAlH$_3$ (top row) and CaAlH$_3$ (bottom row) at the optimal geometries of these two molecules.

The SCGVB description of CaAlH$_3$ at its optimal geometry is dramatically different although there are again three symmetry-equivalent pairs, this time with one pair in each CaHAl bridge. One of the orbitals in each pair (see φ_1 in bottom row of Figure 2) remains semi-localized on the H atom. Its partner (see φ_2 in bottom row of Figure 2) also has significant amplitude on the H atom, suggestive of H^- character, but this orbital extends all of the way from the Al center across the H atom towards the Ca atom. The two orbitals in each pair have an overlap of 0.82 (see Table 3) so that, taken together with the form of orbital φ_2 and a weight of a little more than 99.6% for the perfect pairing mode of spin coupling, this appears to suggest a degree of three-center, two-electron interactions across the polar CaHAl bridges. We observe from the depictions in the bottom row of Figure 2 that orbital φ_8 does still have the basic appearance of an s_- lobe orbital but that φ_7 takes a somewhat different form from that in $MgAlH_3$. Instead of an s_+ lobe function that is heavily deformed towards the Al atom, it has effectively transferred across to the Al atom, taking the form of an Al lobe orbital which is concentrated in the direction that points away from, rather than into, the bridging region. All of this is of course consistent with higher magnitudes for the atomic partial charges in this molecule. The magnitude of the overlap between φ_7 and φ_8 (see Table 3) is relatively small, being 0.21.

Table 2. SCGVB orbital overlaps for $MgAlH_3$ at its optimal CCSD(T)/aug-cc-pVQZ geometry.

	φ_1	φ_2	φ_3	φ_4	φ_5	φ_6	φ_7	φ_8
φ_1	1							
φ_2	0.81	1						
φ_3	0.06	0.13	1					
φ_4	0.13	0.30	0.81	1				
φ_5	0.06	0.13	0.06	0.13	1			
φ_6	0.13	0.30	0.13	0.30	0.81	1		
φ_7	0.10	0.22	0.10	0.22	0.10	0.22	1	
φ_8	0.02	0.02	0.02	0.02	0.02	0.02	0.59	1

Table 3. SCGVB orbital overlaps for $CaAlH_3$ at its optimal CCSD(T)/aug-cc-pVQZ geometry.

	φ_1	φ_2	φ_3	φ_4	φ_5	φ_6	φ_7	φ_8
φ_1	1							
φ_2	0.82	1						
φ_3	0.09	0.15	1					
φ_4	0.15	0.27	0.82	1				
φ_5	0.09	0.15	0.09	0.15	1			
φ_6	0.15	0.27	0.15	0.27	0.82	1		
φ_7	0.12	0.32	0.12	0.32	0.12	0.32	1	
φ_8	0.06	0.05	0.06	0.05	0.06	0.05	−0.21	1

It proves useful at this stage also to examine the results of QTAIM analyses of these SCGVB wave functions. Reasonably linear bond paths from Al to H are observed for $MgAlH_3$ and, moreover, there is an entirely straightforward bond path from Mg to Al, passing through a somewhat ordinary bond critical point. On the other hand, the corresponding analysis for $CaAlH_3$ reveals instead distinctly curved bond paths between the atoms in each CaAlH bridge. Furthermore, instead of a bond critical point and a corresponding bond path the QTAIM analysis detects the presence of a cage critical point between the Ca and Al atoms. (That cage critical point is in effect surrounded by three ring critical points in a plane that is perpendicular to the C_3 axis, with each of the cage critical point to ring critical point directions bisecting a pair of CaAlH bridges.) All in all, visual inspection of the SCGVB solutions as well as the outcome of the QTAIM analysis appears to suggest the absence of any significant degree of direct Ca to Al bonding interactions in this molecule.

The SCGVB calculations, as well as the QTAIM analyses, clearly reveal in a very straightforward and highly visual manner *how* the bonding situation for $CaAlH_3$ at its optimal geometry differs from that for $MgAlH_3$ at its optimal geometry. However, a deeper conundrum remains unanswered: *why* do these two molecules have such different optimal geometries? Seeking a plausible answer, it might seem tempting at this stage to carry out more intimate inspections of the two SCGVB solutions, looking for appropriate differences. However, as we demonstrated above for differences of Coulombic interaction energies between partial charges, it can prove important to attempt to consider separately the change in the angle θ from the replacement of Mg by Ca. Use of the model geometries with optimized values of R_1 and R_2, but with θ fixed at −35° for $MgAlH_3$ and at +4° for $CaAlH_3$, showed in that case that the change from Mg to Ca for a given θ was far less important than the change in geometry. Accordingly, we also carried out SCGVB calculations for $MgAlH_3$ and $CaAlH_3$ at our CCSD(T)/aug-cc-pVQZ model geometries. We find that each of the SCGVB solutions in the present work accounts for almost 99% of the electron correlation that is provided by the corresponding CASSCF(8,8) wave function (Table S6 in the Supporting Information). To a first approximation, the resulting SCGVB active orbitals for $MgAlH_3$ with $\theta = -35°$ (top row of Figure S1 in the Supporting Information) and the overlaps between them (Table S7 in the Supporting Information) are somewhat reminiscent of those for $CaAlH_3$ at its optimal geometry. Similarly, the corresponding results for $CaAlH_3$ with $\theta = +4°$ (Table S8 and bottom row of Figure S1 in the Supporting Information) have a fair amount in common with those for $MgAlH_3$ at its optimal geometry. There are of course some differences that can be linked to the change from $Mg(3s^2)$ to $Ca(4s^2)$ and there is also some evidence for the incorporation of a small degree of $Ca(3d_{z^2})$ character, as might have been anticipated from the study of Fernández et al.,[29] but it does not seem likely that these features could be sufficient on their own to explain the very different geometric preferences of the $MgAlH_3$ and $CaAlH_3$ molecules. Unsurprisingly, we also find that QTAIM analyses of the SCGVB wave functions for each of the model geometries reveals the same basic pattern of critical points and bond paths as for the optimal geometry with the comparable value of θ. (Note that we also found for all four of the CCSD(T)/aug-cc-pVQZ geometries that switching from SCGVB to RHF or CCSD densities made essentially no difference to the resulting patterns of critical points and bond paths.)

It does in fact now turn out that an underlying cause for the rather different optimal geometric arrangements of

$M'AlH_3$ ($M' = Mg$, Ca) might actually have been hidden in plain sight all along. To show that this is the case, it proves instructive to examine the simple energy differences (ΔE) for a given molecule between the model and optimal CCSD(T)/aug-cc-pVQZ geometries, as calculated at various levels of theory using the aug-cc-pVQZ basis set. A selection of such results is reported in Table 4, in which negative values of ΔE for a given molecule indicate that the geometry with $\theta \sim -35°$ is preferred whereas positive values indicate that it is the geometry with $\theta \sim +4°$ which gives the lower energy. (Additional values are reported in Table S9 in the Supporting Information.)

The various energy differences ΔE between the two geometries for a given molecule seem to send a very clear message. Although the optimal geometry for $MgAlH_3$ is preferred at the RHF level by 31.2 kcal/mol, this energy difference is approximately halved when account is taken of non-dynamical electron correlation, whether by means of SCGVB or CASSCF calculations. The incorporation of dynamical electron correlation leads to even smaller values, so that at the CCSD(T) level the energy difference is just 4.6 kcal/mol, *i.e.* less than 15% of the RHF value.

Table 4. Simple energy differences (ΔE) between the $\theta \sim -35°$ and $\theta \sim +4°$ CCSD(T)/aug-cc-pVQZ geometries, as calculated for a given molecule at various levels of theory using the aug-cc-pVQZ basis set. Negative values of ΔE indicate a preference for the $\theta \sim -35°$ geometry.

Method	ΔE (in kcal/mol)	
	$MgAlH_3$	$CaAlH_3$
RHF	31.2	12.2
SCGVB	15.4	0.7
CASSCF(8,8)	15.1	0.6
B3LYP	12.9	−6.8
CCSD	9.0	−16.6
CCSD(T)	4.6	−21.1

The consequences of taking account of electron correlation are even more dramatic in the case of $CaAlH_3$, for which the model geometry with $\theta \sim +4°$ is the preferred one at the RHF level by 12.2 kcal/mol. Taking account of non-dynamical electron correlation, whether by means of SCGVB or CASSCF calculations, reduces this preference by *ca.* 11.5 kcal/mol so that although the model geometry is still the preferred one, the energy difference is now less than 1 kcal/mol. Inclusion of dynamical electron correlation tips the balance further away from the model geometry, so that it is indeed now the optimal geometry which becomes the preferred one, with the value of ΔE reaching −21.1 kcal/mol at the CCSD(T) level. Ultimately it seems for a given molecule that electron correlation, especially dynamical correlation, lowers the energy of the geometries with $\theta \sim -35°$ somewhat more than it does those with $\theta \sim +4°$, probably on account of less spatial separation between electron pairs. For $MgAlH_3$ this leads to a reduction in the preference for the optimal $\theta \sim +4°$ geometry by 26.6 kcal/mol, from 31.2 kcal/mol at the RHF level to 4.6 kcal/mol for CCSD(T). A reduction of this magnitude for $CaAlH_3$, for which ΔE is 12.2 kcal/mol at the RHF level, would already have been enough to switch the energetic ordering of the two geometries. Indeed, the reduction in ΔE for $CaAlH_3$ from RHF to CCSD(T) is larger than that for $MgAlH_3$, being instead 33.3 kcal/mol. Such an extra 6.8 kcal/mol would in fact have been enough in the case of $MgAlH_3$ to make the model geometry with $\theta = -35°$ the preferred one.

Whereas the Coulombic interaction energies consistently favor the geometries with $\theta \sim -35°$ over those with $\theta \sim +4°$, it is the latter which are the preferred ones at the RHF level. As we have seen, the incorporation of electron correlation brings down the energies of the $\theta \sim -35°$ geometries relative to those of the $\theta \sim +4°$ geometries such that the lowering at the CCSD(T) level is sufficient for $CaAlH_3$, but not quite enough in the case of $MgAlH_3$, to switch the energetic ordering of the two geometries. We might though still ponder the magnitude of the differences in the RHF ΔE values: 31.2 kcal/mol for $MgAlH_3$ is reduced to 12.2 kcal/mol for $CaAlH_3$, a difference of 19.0 kcal/mol. The corresponding changes in our simple estimates of the Coulombic interaction energies between RHF VDD atomic partial charges turn out to be 6.9 kcal/mol for $M' \ldots H_3$ and 15.9 kcal/mol for $M' \ldots AlH_3$. These values are at least of the right magnitude.

Certainly it remains true that enhanced Coulombic interaction energies between atomic partial charges could play a role in explanations of the different geometric preferences of these $M'AlH_3$ ($M' = Mg$, Ca) molecules and the same might be said for the rather different bonding arrangements that are revealed by SCGVB theory. Nonetheless, the most important factor ultimately turns out to be electron correlation. Although this is entirely straightforward it is also mildly disappointing because it seems to have denied us a simple highly visual explanation that is based on traditional chemical concepts such as partial charges and differences in the bonding situations.

The strong dominance of the perfect pairing mode of spin coupling in the overall active space spin functions from the SCGVB descriptions of both $MgAlH_3$ and $CaAlH_3$ indicates that these are essentially closed-shell molecules for which it is completely appropriate to use standard coupled-cluster methods based on a closed-shell Hartree-Fock reference. While use of more elaborate coupled-cluster methods and/or even larger basis sets could lead to changes in the energy differences reported in Table 4, the quality of the CCSD(T)/aug-cc-pVQZ combination is sufficient to guarantee that any such changes would be relatively minor and would not affect our explanation of the differences in bonding between $MgAlH_3$ and $CaAlH_3$.

CONCLUSIONS

We were certainly attracted to the suggestions of a link between Coulombic interaction energies and the somewhat different geometric characteristics of the $M'AlH_3$ ($M' = Mg$, Ca) molecules.[6] However, our confidence in such an explanation was dented when we examined also a model geometry for $CaAlH_3$ with an angle, $\theta = +4°$, comparable to that in the optimal geometry of $MgAlH_3$ and, similarly, a model geometry for $MgAlH_3$ with an angle, $\theta = -35°$, comparable to that in the optimal geometry of $CaAlH_3$. Whether we consider changes to the M′…H_3 or M′…AlH_3 Coulombic interaction energies between atomic partial charges, we find the change in θ to be far more important than is the replacement of Mg by Ca.

The SCGVB calculations reported here reveal a rather straightforward description for the optimal geometry of $MgAlH_3$. We may envisage the interaction of the Mg atom with the AlH_3 moiety in terms of the doubly-occupied Mg($3s^2$) orbital splitting into separate s_- and s_+ lobe orbitals that are directed away from and towards, respectively, the Al atom. Unlike the corresponding s_- orbital, which mostly retains its basic form, the s_+ function deforms/distorts significantly towards the Al center, thereby also transferring charge to the AlH_3 moiety. The forms of the various SCGVB active orbitals and the overlaps between them, the dominance of the perfect pairing mode of spin coupling, and the observed pattern of QTAIM critical points and bond paths all point to the presence of direct MgAl and AlH bonding.

Turning now to the SCGVB description for the optimal geometry of $CaAlH_3$, we observe instead of a heavily deformed s_+ lobe function on Ca that there is a lobe function on the Al center which is directed away from, rather than into, the bonding region. In this case, the forms of the various SCGVB active orbitals and the overlaps between them, the dominance of the perfect pairing mode of spin coupling, and the observed pattern of QTAIM critical points and bond paths indicate that the bonding is focused in the polar CaHAl bridges with a degree of three-center, two-electron interactions but no significant degree of direct CaAl bonding.

The various SCGVB calculations certainly show *how* the bonding situation in $CaAlH_3$ differs from that in $MgAlH_3$ when they are both at their optimal geometries but not *why* the geometries differ. That this is so becomes apparent when examining also the SCGVB descriptions of the bonding for the model geometries of $MgAlH_3$ and $CaAlH_3$. Reminiscent of our findings for the Coulombic interaction energies between atomic partial charges, we observe that changing the geometry from $\theta \sim +4°$ to $\theta \sim -35°$ plays a much larger role in determining the nature of the SCGVB solutions than does the replacement of Mg by Ca.

Looking instead at energy differences between model and optimal CCSD(T)/aug-cc-pVQZ geometries, we find that the more standard geometric arrangement with $\theta \sim +4°$ is in fact the preferred one at the RHF/aug-cc-pVQZ level for both of these molecules. It turns out that the incorporation of electron correlation, especially dynamical correlation, brings down the energies of the geometries with $\theta \sim -35°$ relative to those with $\theta \sim +4°$, on account of reduced spatial separation between electron pairs. In the end, the lowering at the CCSD(T) level turns out to be sufficient for $CaAlH_3$, but not quite enough in the case of $MgAlH_3$, to switch the energetic ordering, with the consequence being that these two molecules exhibit dramatically different optimal geometries.

ASSOCIATED CONTENT

Supporting Information. CCSD(T) energies for various geometries of M′AlH_3 and AlH_3; CCSD atomic populations for M′AlH_3; Coulombic interaction energies; RHF, SCGVB and CASSCF energies for M′AlH_3; SCGVB orbitals and orbital overlaps for M′AlH_3 at model geometries; Simple energy differences between $\theta \sim -35°$ and $\theta \sim +4°$ geometries.
This material is available free of charge via the Internet at http://pubs.acs.org.

AUTHOR INFORMATION

Corresponding Author

*Dr. F. E. Penotti. Consiglio Nazionale delle Ricerche
Istituto di Scienze e Tecnologie Chimiche “Giulio Natta”
Via Golgi 19, I–20133 Milano MI, Italy, E-mail:
f.penotti@gmail.com
*Dr. D. L. Cooper, Department of Chemistry, University of Liverpool, Liverpool L69 7ZD, UK, E-mail: dlc@liverpool.ac.uk

Author Contributions

The manuscript was written through contributions of all authors. All authors have given approval to the final version of the manuscript.

Acknowledgment

This research received no external funding.

REFERENCES

(1) Gillespie, R. J. The valence-shell electron-pair repulsion (VSEPR) theory of directed valency. *J. Chem. Educ.* **1963,** *40*, 295.

(2) Gillespie, R. J., The electron-pair repulsion model for molecular geometry. *J. Chem. Educ.* **1970,** *47*, 18.

(3) Bytheway, I.; Gillespie, R. J.; Tang, T.-H.; Bader, R. F. W. Core Distortions and Geometries of the Difluorides and Dihydrides of Ca, Sr, and Ba. *Inorg. Chem.* **1995,** *34*, 2407-2414.

(4) Gillespie, R. J.; Robinson, E. A. Models of molecular geometry. *Chem. Soc. Rev.* **2005,** *34*, 396-407.

(5) Gillespie, R. J. Fifty years of the VSEPR model. *Coord. Chem. Rev.* **2008,** *252*, 1315-1327.

(6) Anusiewicz, I.; Faron, D.; Skurski, P.; Simons, J. Unusual and Conventional Dative Bond Formation by s^2-Lone Pair Donation from Alkaline Earth Metal Atoms to BH_3, AlH_3, and GaH_3. *J. Phys. Chem. A* **2020,** *124*, 5369-5377.

(7) Anusiewicz, I.; Skurski, P. Attaching Be or Mg to BH_3 results in the formation of $BeBH_3$ and $MgBH_3$ molecules capable of forming stable anions. *Chem. Phys. Lett.* **2018,** *698*, 19-23.

(8) Brown, H. C.; Krishnamurthy, S. Forty years of hydride reductions. *Tetrahedron* **1979,** *35*, 567-607.

(9) Calabro, M. Overview on hybrid propulsion. In *EUCASS Proceedings Series – Advances in AeroSpace Sciences, Volume 2*; DeLuca, L. T., Bonnal, C., Haidn, O., Frolov, S. M., Eds.; EDP Sciences: Paris, 2011; pp 353-374.

(10) Zyubin, A. S.; Gorbik, A. A.; Charkin, O. P. Nonempirical calculation of the structure and stability of aluminum magnesium hydrides with consideration of electron correlation. *J. Struct. Chem.* **1989,** *29*, 664-669.

(11) Zyubin, A. S.; Charkin, O. P. Nonempirical calculations of the structure and stability of molecules of calcium aluminum hydrides. *J. Struct. Chem.* **1990,** *31*, 373-378.

(12) Magnusson, E.; Petrie, S. Classical versus Nonclassical Covalent Bonding between the Metal Hydride Radicals MH and M′H_j (MH = HBe, HMg, HCa; M′H_j = Li, BeH, BH_2, Na, MgH, AlH_2, K, CaH, GaH_2). *J. Phys. Chem. A* **2003,** *107*, 6882-6890.

(13) Werner, H.-J.; Knowles, P. J.; Knizia, G.; Manby, F. R.; Schütz, M.; Celani, P.; Györffy, W.; Kats, D.; Korona, T.; Lindh, R.; et al. *MOLPRO, version 2019.2, a package of ab initio programs*. Cardiff, U. K., see www.molpro.net.

(14) Werner, H.-J.; Knowles, P. J.; Knizia, G.; Manby, F. R.; Schütz, M. Molpro: a general-purpose quantum chemistry program package. *WIREs Comput. Mol. Sci.* **2012,** *2*, 242-253.

(15) Werner, H.-J.; Knowles, P. J.; Manby, F. R.; Black, J. A.; Doll, K.; Heßelmann, A.; Kats, D.; Köhn, A.; Korona, T.; Kreplin, D. A.; et al. The Molpro quantum chemistry package. *J. Chem. Phys.* **2020,** *152*, 144107.

(16) Hill, J. G.; Peterson, K. A. Gaussian basis sets for use in correlated molecular calculations. XI. Pseudopotential-based and all-electron relativistic basis sets for alkali metal (K–Fr) and alkaline earth (Ca–Ra) elements. *J. Chem. Phys.* **2017,** *147*, 244106, see www.grant-hill.group.shef.ac.uk/ccrepo/.

(17) Frisch, M. J.; Trucks, G. W.; Schlegel, H. B.; Scuseria, G. E.; Robb, M. A.; Cheeseman, J. R.; Scalmani, G.; Barone, V.; Petersson, G. A.; Nakatsuji, H.; et al. *Gaussian 16, Revision A.03*; Gaussian, Inc.: Wallingford, CT, 2016.

(18) Fonseca Guerra, C.; Handgraaf, J.-W.; Baerends, E. J.; Bickelhaupt, F. M. Voronoi deformation density (VDD) charges: Assessment of the Mulliken, Bader, Hirshfeld, Weinhold, and VDD methods for charge analysis. *J. Comput. Chem.* **2004,** *25*, 189-210.

(19) Lu, T.; Chen, F. Multiwfn: A multifunctional wavefunction analyzer. *J. Comput. Chem.* **2012,** *33*, 580-592.

(20) Pritchard, B. P.; Altarawy, D.; Didier, B.; Gibson, T. D.; Windus, T. L. New Basis Set Exchange: An Open, Up-to-Date Resource for the Molecular Sciences Community. *J. Chem. Inf. Model.* **2019,** *59*, 4814-4820.

(21) Pauncz, R. *The Symmetric Group in Quantum Chemistry*. CRC Press: Boca Raton, 1995.

(22) Schmidt, M. W.; Baldridge, K. K.; Boatz, J. A.; Elbert, S. T.; Gordon, M. S.; Jensen, J. H.; Koseki, S.; Matsunaga, N.; Nguyen, K. A.; Su, S. J.; et al. General atomic and molecular electronic-structure system. *J. Comput. Chem.* **1993,** *14*, 1347-1363.

(23) Gordon, M. S.; Schmidt, M. W. Advances in electronic structure theory: GAMESS a decade later. In *Theory and Applications of Computational Chemistry: The First Forty Years*; Dykstra, C. E., Frenking, G., Kim, K. S., Scuseria, G. E., Eds.; Elsevier: Amsterdam, 2005; pp 1167-1189.

(24) Penotti, F. E. The optimized-basis-set multiconfiguration spin-coupled method for the ab initio calculation of atomic and molecular electronic wave functions. *Int. J. Quantum Chem.* **1993,** *46*, 535-576.

(25) Penotti, F. E. Generalization of the optimized-basis-set multi-configuration spin-coupled method for the ab initio calculation of atomic and molecular electronic wave functions. *Int. J. Quantum Chem.* **1996,** *59*, 349-378.

(26) Penotti, F. E. On the identification of symmetry-forbidden spin subspaces for configurations employing nonorthogonal orbitals. *Int. J. Quantum Chem.* **2000,** *78*, 24-31.

(27) Penotti, F. E. Orbital-orthogonality constraints and basis-set optimization. *J. Comput. Chem.* **2006,** *27*, 762-772.

(28) Bader, R. F. W. *Atoms in Molecules. A Quantum Theory*. Oxford University Press: Oxford, 1990.

(29) Fernández, I.; Holzmann, N.; Frenking, G. The Valence Orbitals of the Alkaline-Earth Atoms. *Chem. Eur. J.* **2020,** *26*, 14194-14210.

TOC Graphic

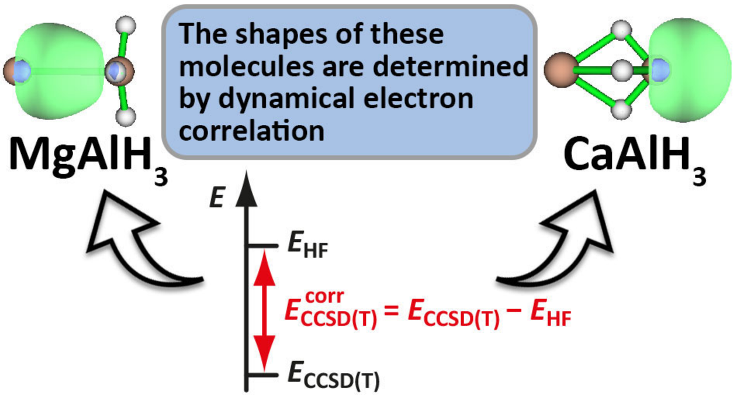
The shapes of these molecules are determined by dynamical electron correlation
MgAlH$_3$
CaAlH$_3$
E
E_{HF}
$E^{corr}_{CCSD(T)} = E_{CCSD(T)} - E_{HF}$
$E_{CCSD(T)}$